Macroporous Electrically Conducting Carbon Networks by Pyrolysis of Isocyanate-Cross-Linked Resorcinol-Formaldehyde Aerogels

Sudhir Mulik, Chariklia Sotiriou-Leventis,* and Nicholas Leventis*

Department of Chemistry, Missouri University of Science and Technology, formerly University of Missouri-Rolla, Rolla, Missouri 65409

Received May 25, 2008. Revised Manuscript Received August 9, 2008

Carbon (C) aerogels are made by pyrolysis of resorcinol-formaldehyde (RF) aerogels under Ar, and they combine electrical conductivity with a high open mesoporosity. However, because macropores are known to facilitate mass transfer, macroporous C-aerogels could be useful for application in separations or as fuel cell and battery electrodes. Macropores are typically incorporated in C-aerogels during gelation of the RF precursors by using either "hard" templating with silica or polystyrene beads, or "soft" templating with surfactants. Here, we report an alternative method, where open macroporosity is introduced by pyrolyzing RF aerogels whose skeletal nanoparticles have been cross-linked covalently with an isocyanate-derived polymer that coats conformally the entire RF framework. The structural, physical, and chemical evolution of the X-RF network was monitored at various stages during pyrolysis by DSC, TGA, SEM, N_2 adsorption porosimetry, and ^{13}C NMR. The accumulated evidence shows that the cross-linker first loses its chemical bonding with the skeletal nanoparticles and then melts, exerting surface tension forces on the RF framework, which cause a partial structural collapse that creates macropores. The xerogel-like internal texture of the macroporous walls is responsible for close contact of the carbon skeletal nanoparticles, resulting in an about 7× lower bulk electrical resistivity of the macroporous material relative to the corresponding mesoporous network, which is obtained by pyrolysis of native (i.e., non-cross-linked) RF aerogels. The new macroporous material was evaluated electrochemically for possible application as an electrode in batteries and fuel cells.

1. Introduction

Carbon (C) aerogels are made by pyrolysis (also referred to as carbonization) of resorcinol-formaldehyde (RF) aerogels at 600−2100 °C under an inert atmosphere.[1] Because C-aerogels combine electrical conductivity with typical aerogel properties such as low density, open mesoporosity (pore sizes less than 50 nm), and high surface area,[2] they are considered for a wide variety of applications ranging from media for separations (e.g., HPLC), to nonreflective panels, to materials for hydrogen storage, to anodes in lithium ion batteries or electrodes for supercapacitors.[3−8]

Providing monolithic carbon or films with either a stereoregular (ordered or periodic) mesoporosity or macroporosity (pore diameters >50 nm) can be beneficial for applications ranging from fuel cell electrodes to photonic crystals.[9−11] Ordered mesoporosity and macroporosity are typically introduced by using either templating agents during gelation, like for example monodispersed beads of polystyrene or silica, which are removed from the wet gels by dissolution in toluene or HF, respectively, or self-assembled surfactant aggregates, which decompose during carbonization of the surrounding RF matrix.[12,13]

In this report, we discuss an alternative method for producing robust macroporous carbon aerogels by pyrolysis of isocyanate-cross-linked RF aerogels. The logic behind our process design was based on prior thermogravimetric analysis data for isocyanate-cross-linked silica aerogels showing complete decomposition of the polymeric cross-linker,[14] thereby suggesting that pyrolysis of RF aerogels in intimate contact with an isocyanate-derived polymer would yield carbon perforated by the voids created from gases evolving

* Corresponding author. E-mail: leventis@mst.edu (N.L.); cslevent@mst.edu (C.S.-L.). Phone: (573) 341-4391(N.L.); (573) 341-4391(C.S.-L.).

(1) (a) Pekala, R. W. *J. Mater. Sci.* **1989**, *24*, 3221–3227. (b) Pekala, R. W.; Alviso, C. T.; Kong, F. M.; Hulsey, S. S. *J. Non-Cryst. Solids* **1992**, *145*, 90–98. (c) Yamamoto, T.; Nishimura, T.; Suzuki, T.; Tamon, H. *J. Non-Cryst. Solids* **2001**, *288*, 46–55. (d) Wen-Cui, Li,; An-Hui, Lu; Schueth, F *Chem. Mater.* **2005**, *17*, 3620–3626.

(2) Al-Muhtaseb, S A.; Ritter, J. A. *Adv. Mater.* **2003**, *15*, 101–114.

(3) Yamamoto, T.; Sugimoto, T.; Suzuki, T.; Mukai, S. R.; Tamon, H. *Carbon* **2002**, *40*, 1345–1351.

(4) (a) Pekala, R. W.; Farmer, J. C.; Alviso, C. T.; Tran, T. D.; Mayer, S. T.; Miller, J. M.; Dunn, B. *J. Non-Cryst. Solids* **1998**, *225*, 74–80. (b) Jurewicz, K.; Frackowiak, E.; Beguin, F. *J. Power Sources* **2001**, *96*, 270.

(5) Kabbour, H.; Baumann, T. F.; Satcher, J. H., Jr.; Saulnier, A.; Ahn, C. C. *Chem. Mater.* **2006**, *18*, 6085–6087.

(6) Merzbacher, C. I.; Meier, S. R.; Pierce, J. R.; Korwin, M. L. *J. Non-Cryst. Solids* **2001**, *285*, 210–215.

(7) Chan, K.; Ding, J.; Ren, J.; Cheng, S.; Tsang, K. *J. Mater. Chem.* **2004**, *14*, 505–516.

(8) (a) Biesmans, G.; Mertens, A.; Duffours, L.; Woignier, T.; Phalippou, J. *J. Non-Cryst. Solids* **1998**, *225*, 64–68. (b) Sakintuna, B.; Yueruem, Y. *Ind. Eng. Chem. Res.* **2005**, *44*, 2893–2902.

(9) Liu, R.; Shi, Y.; Wan, Y.; Meng, Y.; Zhang, F.; Gu, D.; Chen, Z.; Tu, B.; Zhao, D. *J. Am. Chem. Soc.* **2006**, *128*, 11652–11662.

(10) Baumann, T. F.; Satcher, J. H. *J. Non-Cryst. Solids* **2004**, *350*, 120–125.

(11) Perpall, M. W.; Perera, K. P. U.; DiMaio, J.; Ballato, J.; Foulger, S. H.; Smith, D. W. J. *Langmuir* **2003**, *19*, 7151–7156.

(12) Gierszal, K. P.; Jaroniec, M. *J. Am. Chem. Soc.* **2006**, *128*, 10026–10027.

(13) Tanaka, S.; Katayama, Y.; Tate, M. P.; Hillhouse, H. W.; Miyake, Y. *J. Mater. Chem.* **2007**, *17*, 3639–3645.

(14) (a) Leventis, N.; Sotiriou-Leventis, C.; Zhang, G.; Rawashdeh, A.-M. M. *Nano Lett.* **2002**, *2*, 957–960. (b) Zhang, G.; Dass, A.; Rawashdeh, A.-M. M.; Thomas, J.; Counsil, J. A.; Sotiriou-Leventis, C.; Fabrizio, E. F.; Ilhan, F.; Vassilaras, P.; Scheiman, D. A.; McCorkle, L.; Palczer, A.; Johnston, J. C.; Meador, M. A. B.; Leventis, N. *J. Non-Cryst. Solids* **2004**, *350*, 152–164.

10.1021/cm801428p CCC: $40.75
Published on Web 11/01/2008

during decomposition of the cross-linker. As it turns out, our working hypothesis was only partially correct. First, cross-linking of RF wet gels proceeds smoothly in analogy to silica. The process stabilizes the RF skeletal framework against shrinkage, yielding sturdy lightweight materials with densities lower even than those of their native counterparts. Subsequently, during pyrolysis, the cross-linker melts before it decomposes, thereby exerting surface tension forces, which transform the mesoporous RF network into a macroporous one that upon carbonization is converted to a new electrically conducting material with morphology and properties different from those of typical carbon aerogels obtained from native (non-cross-linked) RF aerogels. The new macroporous carbon aerogels were evaluated electrochemically for possible application as electrode materials in batteries and fuel cells.

2. Experimental Section

2.1. Materials. Formaldehyde (37% aqueous solution methanol stabilized) and acetone (anhydrous) were used as received from Aldrich Chemical Co. Acetonitrile (ACS reagent grade) and hydrochloric acid (12.1 N) were purchased from Fisher Scientific. Resorcinol received from Aldrich was sublimed before use. Triethylamine was obtained from Acros Chemicals and was further purified by distillation over calcium hydride. Isocyanate cross-linkers Desmodur N3200 and Desmodur N3300 were obtained courtesy of Bayer Corporation (Pittsburgh, PA). Siphon grade CO_2 was obtained from BOC Gases, Murray Hill, NJ, supplied locally by Ozarc Gases. For electrochemistry, a platinum disk working electrode (2.0 mm diameter, 0.0314 cm^2) and a Ag/AgCl/aqueous KCl (3 M) reference electrode were purchased from CH Instruments, Inc. (Austin, TX). The counter electrode was constructed from a Pt mesh (Aldrich). Disk working electrodes were polished successively with 6, 3, and 1 μm diamond paste (Struers Inc., Westlake, OH), washed with water and acetone, and air-dried. Ferrocene (Aldrich-sublimed) was used as a reference redox system. Platinum electrodeposition was carried out using potassium tetrachloroplatinate (Aldrich) as the Pt source. Tetrabutylammonium perchlorate (TBAP) was used as supporting electrolyte and was prepared as described previously.[15]

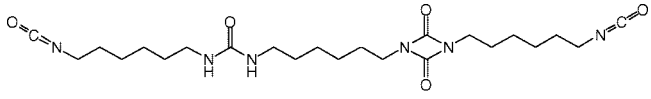

N3200

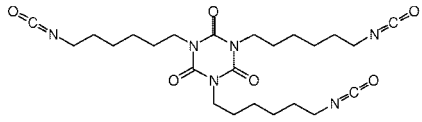

N3300A

Preparation of Native RF Aerogels. RF wet gels with a 1:2 mol R:F ratio were prepared by mixing at room temperature solution "A" containing 0.337 g (0.003 mol) of resorcinol, 0.477 mL (0.006 mol) of the commercially available formaldehyde solution, and 11.5 mL CH_3CN, with solution "B" containing 0.636 mL of CH_3CN and 0.03 mL (0.363 mmol) of concentrated HCl as catalyst, as we reported recently.[16] The mixture (sol) was poured into molds (either Wheaton polypropylene Omni-Vials, part No. 225402, 1.04 cm in diameter, or 10 mL AirTite Norm-Ject syringes without needles supplied by Fisher) and gelation occurs within 2 h at room temperature or in about 10 min at 80 °C. Typically, the resulting gels were aged in their molds at room temperature for 24 h, and subsequently they were washed with acetone (3×, 8 h, 4× the volume of the gel each time) and they were dried in an autoclave with liquid CO_2, taken out at the end supercritically to obtain native RF aerogels.

Preparation of Isocyanate-Cross-Linked RF Aerogels. The cross-linking solution was prepared by mixing 11 g of isocyanate (Desmodur N3200 or Desmodur N3300A) in 94 mL of anhydrous acetone with or without 0.117 mL (0.1 wt % over the total weight of the isocyanate plus the solvent) of anhydrous triethylamine (TEA) as catalyst. After wet gels were washed with acetone (3×, 8 h, 4× the volume of the gel each time), they were placed in the cross-linking solution and the isocyanate cross-linker was allowed to diffuse into the pores of the wet gels and to equilibrate for 24 h. After heating at 55 °C for another 24 h, the containers were cooled to room temperature and gels were removed and placed in fresh acetone. After further washing with acetone (3 ×, 8 h, 4 × the volume of the gel each time) wet gels were dried in an autoclave with liquid CO_2, taken out at the end supercritically to form cross-linked RF aerogels (X-RF aerogels).

Preparation of polyurea aerogels. Control polyurea aerogels were prepared by mixing at room temperature 11 g of Desmodur N3300A, 94 mL of acetonitrile or acetone, 0.19 mL of distilled water and 0.35 mL (0.3 wt % over the total weight of Desmodur N3300A plus the solvent) of triethylamine (TEA). The resulting sol gels within 30 min. After 24 h of aging, wet polyurea gels were washed with acetone (3×, 8 h, 4× the volume of the gel each time) and dried in an autoclave with liquid CO_2, taken out supercritically.

Preparation of Carbon Aerogels. Native RF aerogels and their X-RF counterparts cross-linked with either Desmodur N3200 or Desmodur N3300A were pyrolyzed at 800 °C for 3 h in a tube furnace under a flowing stream of Ar. Prior to pyrolysis, the tube was purged with Ar for 10 min before heating was initiated at a rate of 5 °C min^{-1}. At the end of the heating period, the power to the furnace was disconnected and the tube was allowed to cool slowly back to room temperature under flowing Ar. For control purposes, pyrolysis of X-RF aerogels was also conducted at 200, 250, and 300 °C under the same conditions.

2.2. Methods. Supercritical fluid (SCF) CO_2 drying was carried out using an autoclave (SPI-DRY Jumbo Supercritical Point Drier, SPI Supplies, Inc., West Chester, PA). Bulk densities were calculated from the weight and the physical dimensions of the samples. In cases of irregularly shaped samples, where measurement of the physical dimensions was not possible, sample volumes were determined using the mercury displacement method. Skeletal densities were determined by helium pycnometry using a Micromeritics AcuuPyc II 1340 instrument. Mesoporous surface areas and pore size distributions were measured by nitrogen adsorption/desorption porosimetry using a Quantachrome Autosorb-1 surface area/pore distribution analyzer. Samples for surface area and skeletal density determination were degassed at 80 °C for 24 h before analysis. Scanning electron microscopy (SEM) and energy-dispersive X-ray spectroscopy (EDS) were conducted with a Hitachi S-4700 field emission microscope. RF aerogel samples for SEM were sputter-coated with Ag/Pd for 2 min to avoid charging; that treatment was not necessary for carbon aerogels, because they were electrically conducting. Chemical characterization of native as well as cross-linked RF aerogels was based on IR and solid state ^{13}C NMR. Infrared spectra were obtained in KBr pellets using a Nicolet-FTIR model 750 Spectrometer. Solid ^{13}C NMR spectra were

(15) (a) Leventis, N.; Gao, X. *J. Electroanal. Chem.* **2001**, *500*, 78–94. (b) Leventis, N.; Oh, W. S.; Gao, X.; Rawashdeh, A.-M. M. *Anal. Chem.* **2003**, *75*, 4996–5005.

(16) Mulik, S.; Sotiriou-Leventis, C.; Leventis, N. *Chem. Mater.* **2007**, *19*, 6138–6144.

Scheme 1. Synthesis of Native and Isocyanate Cross-Linked Resorcinol-Formaldehyde Aerogels (RF and X-RF, respectively)

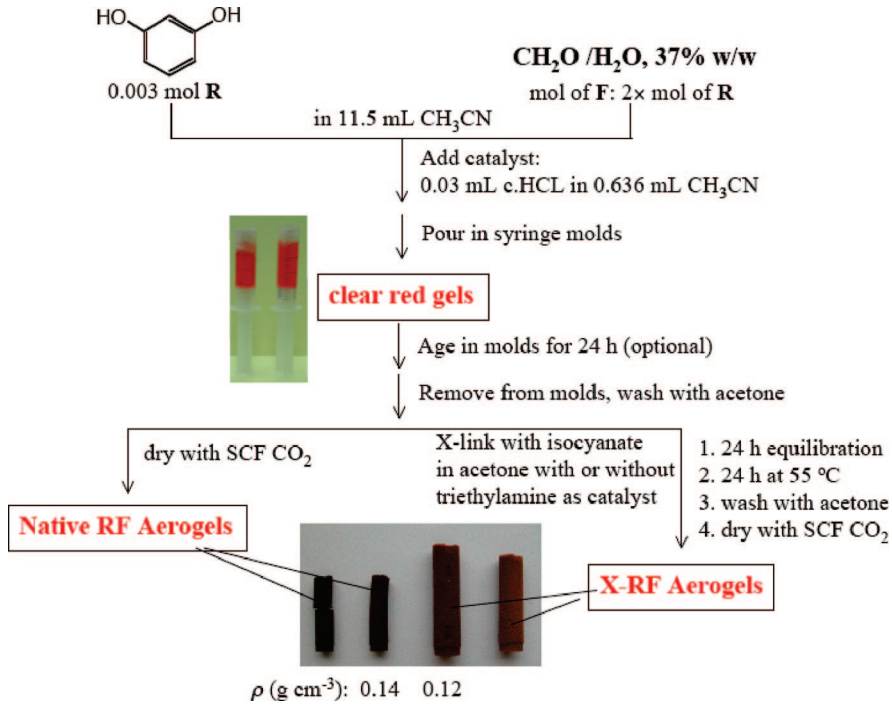

obtained with samples ground in fine powders on a Bruker Avance 300 spectrometer with 75.475 MHz carbon frequency, using magic angle spinning (5 kHz) with broadband proton suppression and the CPMAS TOSS pulse sequence for spin sideband suppression. ^{13}C NMR spectra were externally referenced to the carbonyl of glycine (196.1 ppm relative to tetramethylsilane). Thermogravimetric analysis (TGA) was conducted under nitrogen with a TA Instrument, model Hi-Res-TGA 2950 using a heating rate of 10 °C min^{-1}. Modulated differential scanning calorimetry (MDSC) was conducted under nitrogen from 30 to 300 °C with a TA Instrument model 2920 apparatus at a heating rate of 10 °C min^{-1}. The mass of each sample was approximately 8−12 mg.

Four-point-probe conductivity measurements were conducted on flat surfaces of rectangular blocks of carbon aerogel samples (made with a fine sand paper) using an Alesis contact probe station model CPS −06 with a Cascade Microtech electrode model C4S-44/5S. The reliability of the probe was confirmed with silicon wafers and indium−tin-oxide coated glass slides of known sheet resistance. Electrochemical evaluation of carbon aerogels was conducted using standard millielectrode cyclic voltammetry with a Pt disk electrode (2 mm diameter), an EG&G 263A potentiostat controlled by the EG&G model 270/250 software and ferrocene (3 mM) in CH_3CN/0.1 M TBAP as a reference redox system. Platinum electrodeposition using carbon aerogels as working electrodes was conducted potentiostatically (at 0.0 V versus aq. Ag/AgCl) from a potassium tetrachloroplatinate solution (II) (3 mM) in CH_3CN/0.1 M TBAP (using a minimal amount of water in order to dissolve K_2PtCl_4) and the charge passed was calculated by integration of the current−time trace recorded on a Kipp & Zonen X−Y recorder.

3. Results and Discussion

Native RF Aerogels and Their Cross-Linking with Isocyanates. Native RF wet gels were prepared using our recently reported time-efficient HCl-catalyzed route in CH_3CN (Scheme 1).[16] By that method gelation takes place at room temperature within 2 h (or in 10 min at 80 °C), as opposed to the usual aqueous base-catalyzed gelation that requires a week-long incubation at 80 °C.[1] Native RF aerogels were obtained

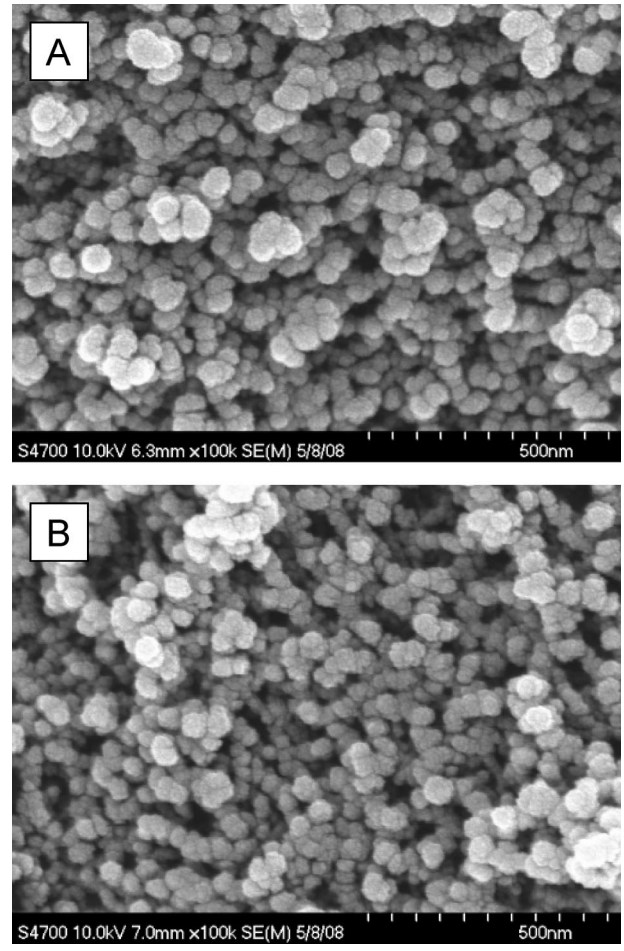

Figure 1. Scanning electron microscopy (SEM) of (A) a native RF aerogel, and (B) a Desmodour N3300A tri-isocyanate cross-linked (X-RF) aerogel, prepared according to Scheme 1.

Table 1. Physical Characterization of Native and Isocyanate Crosslinked RF Aerogels Processed under Various Conditions

cross-linker and conditions	monolith diam.[a,b](cm)	monolith diam. shrinkage %	bulk density [b] (ρ_b, g cm^{-3})	skeletal density [c] (ρ_s, g cm^{-3})	% polymer (wt/wt)	porosity, Π (% void space) [d]	BET surf. area, σ [avg. pore diam.[e]] (m^2g^{-1}[nm])	particle diam.[f] (nm)
	0.65 ± 0.02	39	0.136 ± 0.008	1.363 ± 0.056		90	318 [14.7; 83.3]	13.8
N3200	0.83 ± 0.02	21	0.135 ± 0.005	1.288 ± 0.032	52	90	363 [7.5; 73.1]	12.8
N3200 + 0.1% w/w TEA	0.89 ± 0.01	15	0.126 ± 0.004	1.234 ± 0.017	58	90	396 [8.3; 72.0]	12.3
N3300A	0.82 ± 0.01	22	0.125 ± 0.006	1.323 ± 0.039	46	91	387 [8.4; 74.9]	11.7
N3300A + 0.1% w/w TEA	0.91 ± 0.01	13	0.120 ± 0.005	1.196 ± 0.023	59	90	396 [7.8; 75.7]	12.7

[a] Mold diameter = 1.04 cm. [b] Average of 3 samples. [c] One sample, average of 50 measurements. [d] Porosity, $\Pi = [[1/(\rho_b) - 1/(\rho_s)]/(1/\rho_b)] \times 100$. [e] By the $4V_{Total}/\sigma$ method, where V_{Total} is the mass specific total pore volume and has been calculated by two methods, hence the two numbers cited for the average pore diameter: first automatically by the system software from a single point volume measurement of the N_2 adsorbed, and second manually from the bulk and skeletal densities via $V_{Total} = (1/\rho_b) - (1\rho_s)$. [f] Particle diameter = $6/\rho_s\sigma$.

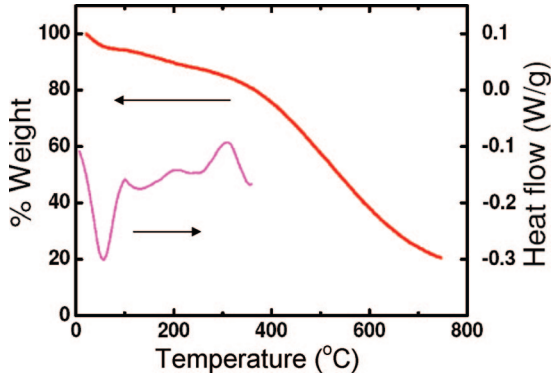

Figure 2. Thermogravimetric analysis (TGA) and differential scanning calorimetry (DSC) both under N_2 of native RF aerogels (heating rate: 10 °C/min). (Exo is up.)

by SCF CO_2 drying of RF wet gels, and microscopically they

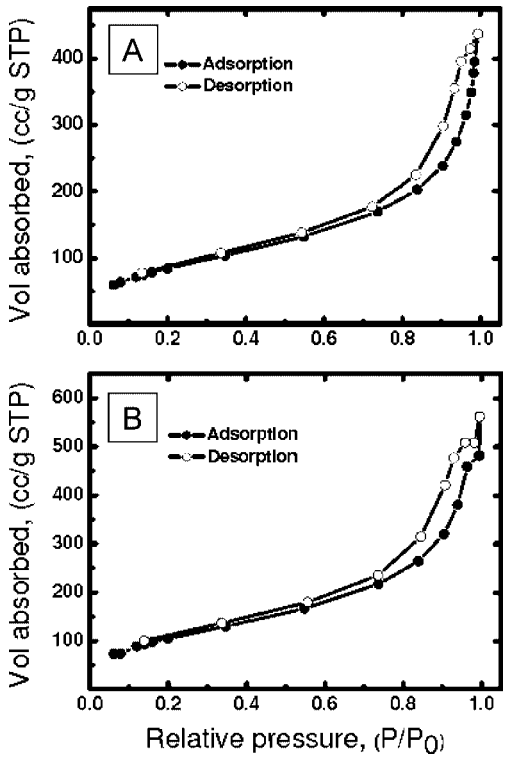

Figure 3. Nitrogen sorption porosimetry. (A) Adsorption−desorption isotherms for a native RF aerogel ($\rho_b = 0.136 \pm 0.008$ g cm^{-3}; BET surface area = 318 m^2 g^{-1}). (B) Adsorption−desorption isotherms for a X-RF aerogel cross-linked with Desmodur N3300A in the presence of TEA ($\rho_b = 0.120 \pm 0.005$ g cm^{-3}; BET surface area = 396 m^2 g^{-1}).

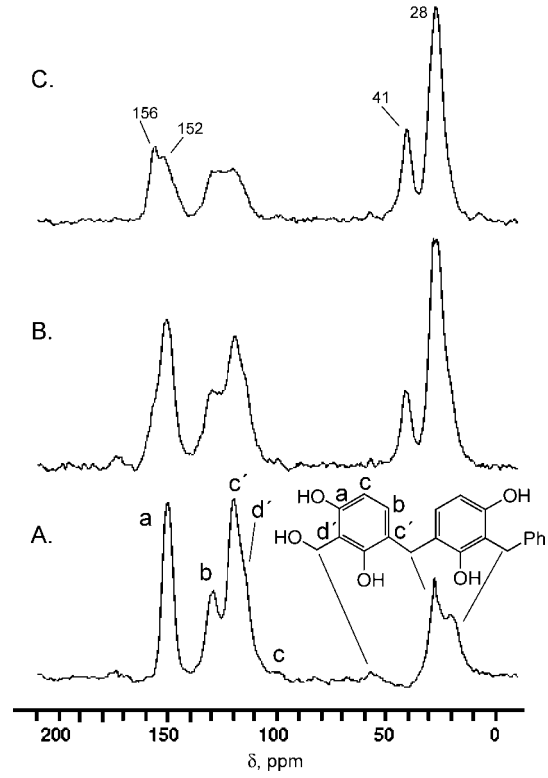

Figure 4. Solid ^{13}C CPMAS NMR of (A) acid-catalyzed native RF aerogel, (B) a X-RF aerogel sample cross-linked with Desmodur N3300A without catalyst, and (C) a X-RF aerogel sample cross-linked with Desmodur N3300A in the presence of TEA. (For pertinent materials characterization data refer to Table 1.)

are indistinguishable from typical base-catalyzed silica aerogels,[16] consisting of a pearl-necklace-like network of secondary particles (40−70 nm in diameter), which in turn consist of primary particles (10−12 nm in diameter, see Figure 1A). Furthermore, by TGA native RF aerogels show a mass loss of 6% up to 80 °C, with a simultaneous DSC endotherm at 65 °C (Figure 2). This behavior is identical to the one exemplified by native silica aerogels and indicates gelation water remaining adsorbed (presumably through hydrogen bonding) on the nanoparticles even after the SCF CO_2 drying process. Water remaining adsorbed on silica has been used extensively for cross-linking the skeletal nanoparticles with polyurea;[14] for this, di- or tri-isocyanates are introduced in the mesopores and they first get anchored to the skeletal silica network via carbamates formed by reaction with surface silanols. Subsequently, dangling isocyanates are hydrolyzed by the gelation water remaining

Scheme 2. Cross-Linking of an RF Network with and without TEA as Cross-Linking Catalyst

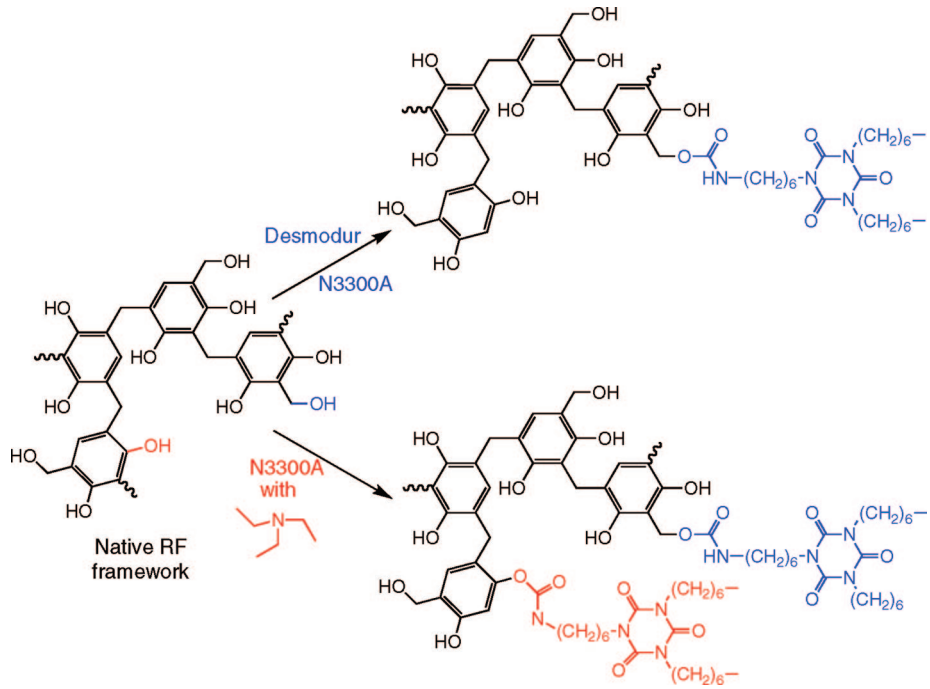

adsorbed on the skeletal silica framework yielding amines, which in turn react with more isocyanate in the mesopores, resulting in interparticle polymeric bridges of polyurea.[14]

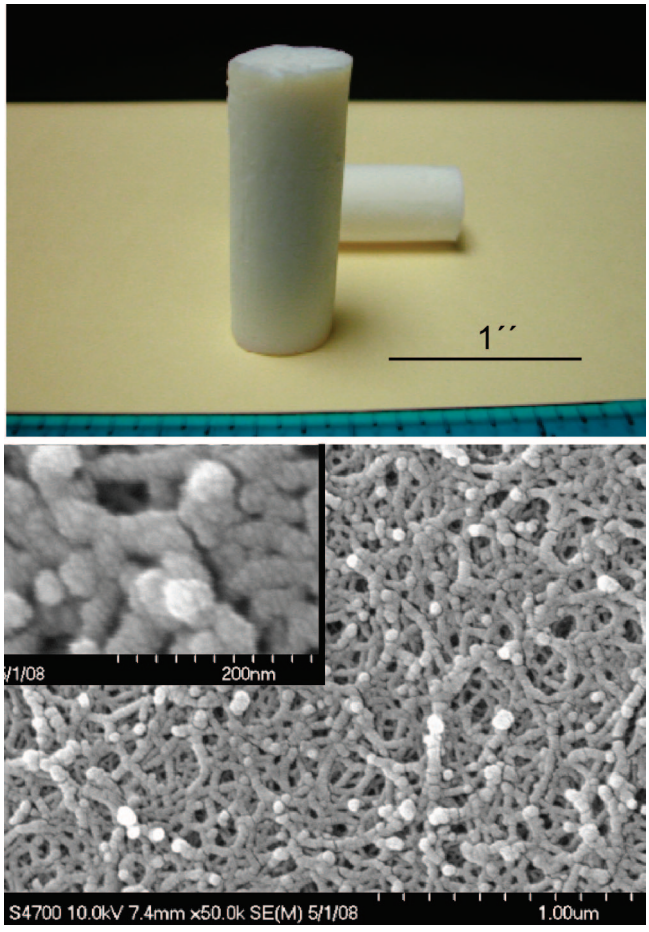

Figure 5. (A) Photograph and (B) SEM of a polyurea aerogel sample prepared by gelation of Desmodur N3300A in acetone/water in the presence of TEA.

Because the surface of the RF particles has both hydroxyls (from resorcinol and from terminal -CH_2OH groups) and adsorbed water, a similar cross-linking chemistry to that working on silica was adopted for RF aerogels (Scheme 1): RF wet gels were placed in acetone solutions of Desmodur N3200 (a diisocyanate) or Desmodur N3300A (a triisocyanate) and left to equilibrate for 24 h at room temperature before being heated at 55 °C for another 24 h. In a preferred modified version of this process, the cross-linking reaction was catalyzed by triethylamine (TEA). The amount of the catalyst is important, because it turns out that a small excess of catalyst in the presence of a low concentration of residual water in the solvent catalyzes the gelation of the cross-linker itself. For example, 0.1% wt/wt of TEA catalyzes cross-linking, but 0.3% wt/wt TEA catalyzes gelation of N3300A as well (see Experimental Section and section 3.2 below). After the cross-linking process, unreacted isocyanate was removed from the mesopores by washing with acetone and cross-linked wet gels were dried into cross-linked X-RF aerogels in a similar fashion as their native counterparts. Key properties of RF and X-RF aerogels are cited in Table 1.

Both native and cross-linked RF aerogels shrink during the SCF drying process. Shrinkage is quantified by comparing a linear dimension such as the diameter of monolithic samples relative to their molds. As shown by the photographs of Scheme 1, native RF aerogels shrink significantly (up to 39%), whereas all cross-linked samples shrink much less (Table 1). Furthermore, cross-linking in the presence of a catalyst (TEA) produces X-RF aerogels that shrink even less (13−15%) than X-RF aerogels prepared with no catalyst (21−22%). The latter is attributed to a more extensive cross-linking (see same section below).

Thermogravimetric analysis is not reliable for the determination of the amount of the material uptaken during cross-linking. In contrast to cross-linked inorganic aerogels (e.g., silica, rare earths, vanadia), where the backbone is thermally

Table 2. Material Characterization Data of Polyurea Aerogels Derived from Desmodur N3300A.

bulk density [a,b] (ρ_b, g cm^{-3})	skeletal density [c] (ρ_s, g cm^{-3})	porosity, Π (% void space) [d]	BET surf. area, σ [avg pore diam. [e]] (m^2 g^{-1}[nm])	% shrinkage
0.144 ± 0.024	1.201 ± 0.005	88	189 [45.3]	20.4

[a] Mold diameter = 2.0 cm. [b] Average of 3 samples. [c] One sample, average of 50 measurements. [d] Porosity, $\Pi = [[1/(\rho_b) - 1/(\rho_s)]/(1/\rho_b)] \times 100$. [e] By the $4V_{Total}/\sigma$ method, where $V_{Total} = (1/\rho_b) - (1/\rho_s)$.

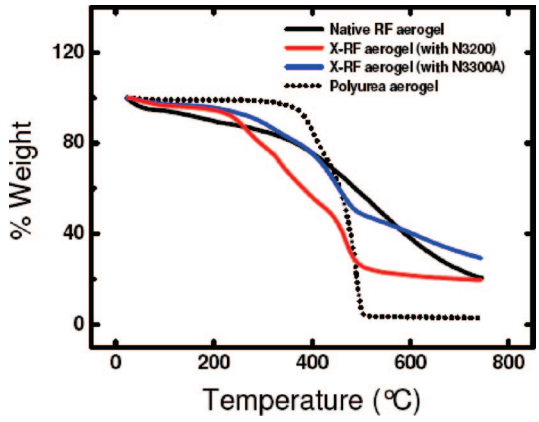

Figure 6. Thermogravimetric analysis under N_2 of a native RF, two X-RF samples, one cross-linked with Desmodur N3200 di-isocyanate and one with Desmodur N3300A tri-isocyanate, and a polyurea aerogel, as indicated. (Heating rate: 10 °C min^{-1}.)

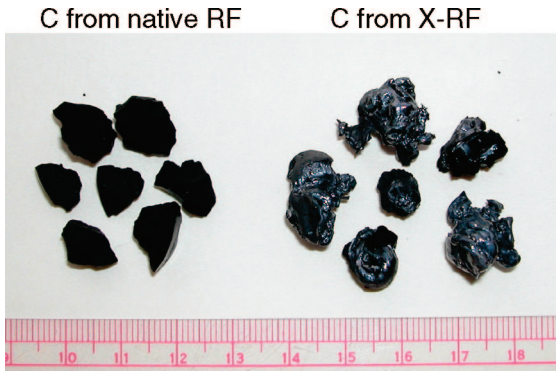

Figure 7. Photographs of carbon aerogels prepared by pyrolysis at 800 °C under Ar of native RF aerogels and of X-RF aerogels prepared using Desmodur N3300A tri-isocyanate and TEA.

stable,[14,17] in X-RF aerogels, both the RF backbone and the material uptaken by cross-linking are heat-sensitive and the decomposition of the latter is convoluted with the decomposition of the former. Instead, the amount of material uptaken by the cross-linking process is calculated via eq 1, which is based on the relative density and volume data of the native versus the X-RF samples (diameters and densities in eq 1 refer to those of monoliths). The results are included in Table 1 (see % polymer wt/wt column).

$$\text{polymer weight percent} = \left[1 - \left[\left(\frac{\text{diameter}_X}{\text{diamter}_{\text{native}}}\right)^3 \times \left(\frac{\rho_X}{\rho_{\text{native}}}\right)\right]^{-1}\right] \times 100 \quad (1)$$

Despite the fact that X-RF aerogels consist of 46−59% wt/wt new material uptaken during treatment with isocyanate, their bulk density is generally lower than that of the native

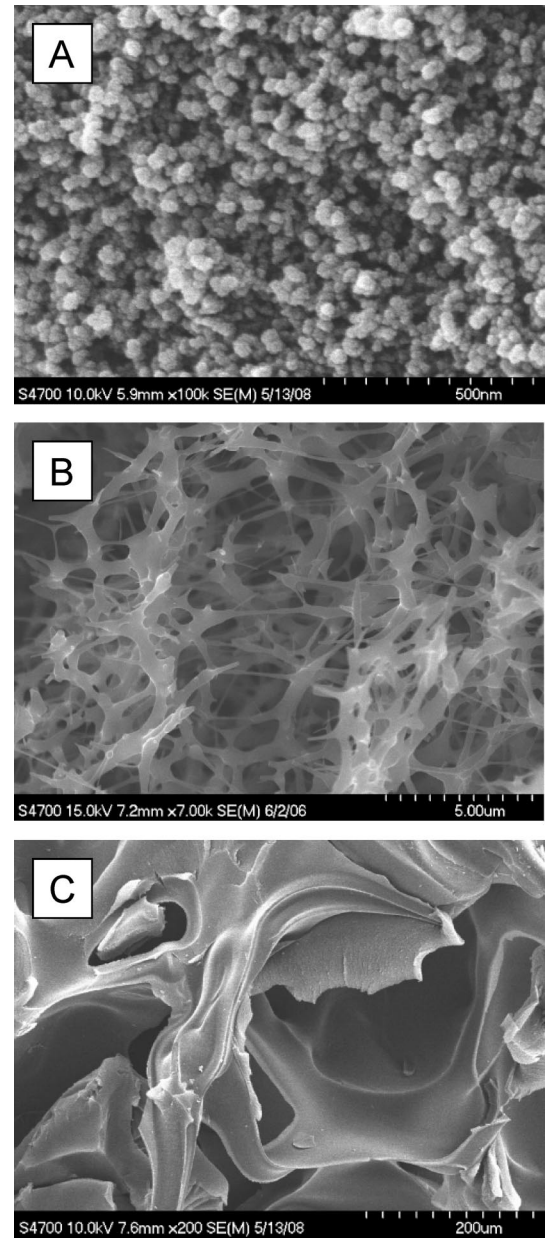

Figure 8. SEM of (A) carbon aerogels made by pyrolysis of native RF aerogels, (B) X-RF aerogels cross-linked with Desmodur N3300A tri-isocyanate, (C) and X-RF aerogels cross-linked with Desmodur N3200 di-isocyanate. (Notice the different magnifications and length scales.)

RF aerogel samples (Table 1); this is attributed directly to the fact that X-aerogels shrink less. For the same reason, the porosity of all samples, either native or cross-linked,

(17) (a) Leventis, N. *Acc. Chem. Res.* **2007**, *40*, 874–884. (b) Katti, A.; Shimpi, N.; Roy, S.; Lu, H.; Fabrizio, E. F.; Dass, A.; Capadona, L. A.; Leventis, N. *Chem. Mater.* **2006**, *18*, 285–296. (c) Leventis, N.; Sotiriou-Leventis, C.; Mulik, S.; Dass, A.; Schnobrich, J.; Hobbs, A.; Fabrizio, E. F.; Luo, H.; Churu, G.; Zhang, Y.; Lu, H. *J. Mater. Chem.* **2008**, *18*, 2475–2482. (d) Leventis, N.; Vassilaras, P.; Fabrizio, E.; Dass, A. *J. Mater. Chem.* **2007**, *17*, 1502–1508.

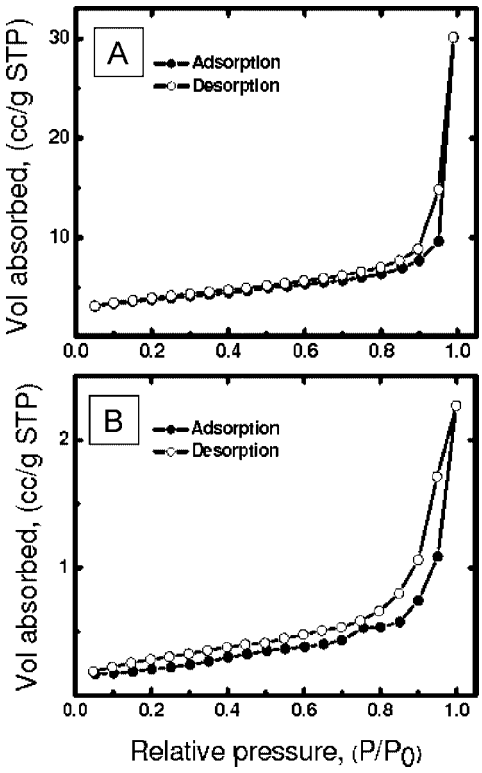

Figure 9. Nitrogen sorption porosimetry. (A) Adsorption−desorption isotherms for a C-aerogel made from a native RF aerogel ($\rho_b = 0.138 \pm 0.024$ g cm^{-3}; BET surface area = 626 m^2 g^{-1}). (B) Adsorption−desorption isotherms for a C-aerogel prepared from a X-RF aerogel cross-linked with Desmodur N3300A in the presence of TEA ($\rho_b = 0.254 \pm 0.082$ g cm^{-3}; BET surface area = 17 m^2 g^{-1}).

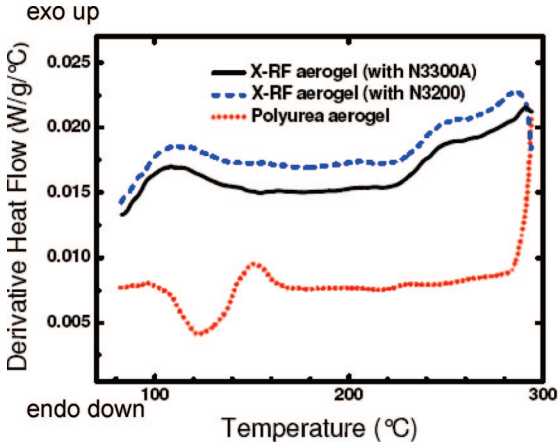

Figure 10. Differential scanning calorimetry (DSC) under N_2 at 10 °C min^{-1} of two X-RF samples, one cross-linked with Desmodur N3200 di-isocyanate and one with Desmodur N3300A tri-isocyanate, and a polyurea aerogel, as indicated.

remains about constant. Microscopically, X-RF aerogels show an identical morphology to the native samples (Figure 1B), signifying that the isocyanate-derived material is added conformally on the skeletal nanoparticles, as designed. According to SEM, both native and cross-linked samples include pores in the threshold of mesopores and macropores (50 nm range). N_2 sorption isotherms do not reach saturation up to the maximum pressure allowed by the instrument (1 atm), but they do show hysteresis (a characteristic feature of type IV and type V isotherms) and from the lower pressure part of the curves we conclude that they are indeed type IV isotherms characterizing mesoporous materials (Figure 3). The internal surface area, σ, is derived from the linear lower partial pressure part of the isotherms according to the Brunauer, Emmett, Teller (BET) method,[18] and results are also cited in Table 1. Cross-linked samples have up to 20% higher surface areas than their native counterparts. This is opposite to what has been observed before with any other kind of polymer cross-linked aerogels, and most probably it is due to two reasons: (a) the fact that X-RF aerogels experience significantly less drying shrinkage than their native counterparts; and (b) the cross-linker-derived coating is porous. Average particle diameters were calculated on the basis of skeletal density and BET surface area data (see footnote f in Table 1)[19] and they all fall in the 12−14 nm range, in agreement with the primary particles observed by SEM. Average pore diameters have been calculated via the $4V_{Total}/\sigma$ method using as V_{Total} either a single-point measurement of the (highest) volume of N_2 adsorbed along the isotherm, or calculated from the bulk and skeletal density of the material (see footnote e in Table 1). The single-point method tends to underestimate V_{Total}, particularly when isotherms do not reach saturation.[14] The average pore diameters via V_{Total} calculated using the densities method fall in the 70−80 nm range, in agreement with SEM.

Chemical changes brought about by the cross-linking process have been followed with CPMAS solids ^{13}C NMR spectroscopy. Figure 4A shows the ^{13}C NMR spectrum of a typical native RF sample with peak assignment as shown.[16] Upon cross-linking with Desmodur N3300A (Figure 4B), we observe the characteristic pattern of the hexamethylene moiety of N3300A with a resonance at 41 ppm and a stronger one at 28 ppm, overlapping with the resonance of the methylene bridges in RF. If there were any unreacted isocyanate groups from N3300A they should appear at 128 ppm overlapping with the 130/120 ppm pattern of RF.[14,16] However, no unreacted isocyanate at 2273−2000 cm^{-1} (N═C═O stretch[24]) has been detected by IR (shown in the Supporting Information). In fact, the characteristic pattern of RF in the 120−130 ppm range remains unchanged after cross-linking with no catalyst (Figure 4B), meaning that interaction of the isocyanate with the RF framework has taken place only at the terminal -CH_2OH groups on its surface. Finally, the sharp, symmetric resonance of the phenolic carbon (C-OH) of RF at 151 ppm (Figure 4A) is expected to partially overlap with the isocyanurate carbonyls at ∼148 ppm, and both the carbamate and the urea carbonyls at 157 pm and at 159 ppm, respectively.[14] Indeed, after cross-linking (Figure 4B), the 151 ppm peak becomes broad and asymmetric with shoulders at 158 ppm (carbamate and urea) and at 148 ppm (isocyanurate of N3300A). By using TEA as a catalyst, the ^{13}C NMR spectrum changes drastically (Figure 4C). The relative intensity of the hexamethylene groups of N3300A is increased, meaning a higher incorporation of N3300A derived polymer, in agreement with the

(18) Brunauer, S.; Emmett, P. H.; Teller, E. *J. Am. Chem. Soc.* **1938**, *60*, 309.
(19) Hüsing, N.; Schubert, U.; Mezei, R.; Fratzl, P.; Riegel, B.; Kiefer, W.; Kohler, D.; Mader, W. *Chem. Mater.* **1999**, *11*, 451–457.
(20) Fricke, J.; Reichenauer, G. *J. Non-Cryst. Solids* **1987**, *95−96*, 1135–1142.

Table 3. Characterization of Carbon Aerogels Derived from Native RF and X-RF Aerogels

C-aerogel derived by pyrolysis of	bulk density [a] (ρ_b, g cm^{-3})	skeletal density [b] (ρ_s, g cm^{-3})	porosity, Π (% void space)	BET surf. area, σ [avg pore diam. [c]] (m^2g^{-1} [nm])	particle diameter (nm)	bulk resistivity ($\mu\Omega$ cm)
native RF aerogel	0.138 ± 0.024	2.146 ± 0.121	93	626 [43]	4.47	6.8×10^6
X-RF-N3200 aerogel	0.218 ± 0.090	1.814 ± 0.022	88	2.3 [7018]	(1438) [d]	[e]
X-RF-N3300A aerogel	0.254 ± 0.082	1.866 ± 0.011	86	17 [800]	(189) [d]	5.0×10^5

[a] Average of 3 samples. [b] One sample, average of 50 measurements. [c] Average pore diameter $= 4V_{Total}/\sigma$, where $V_{Total} = (1/\rho_b) - (1/\rho_s)$. [d] In those cases, "particle" should be rather taken to mean "elementary building block." Numbers in parentheses are given for comparative purposes only, because the macroporous aerogel networks do not consist of particles. [e] Because of the extreme fragility of those materials, fabrication of rectangular blocks for electrical measurements was not easy.

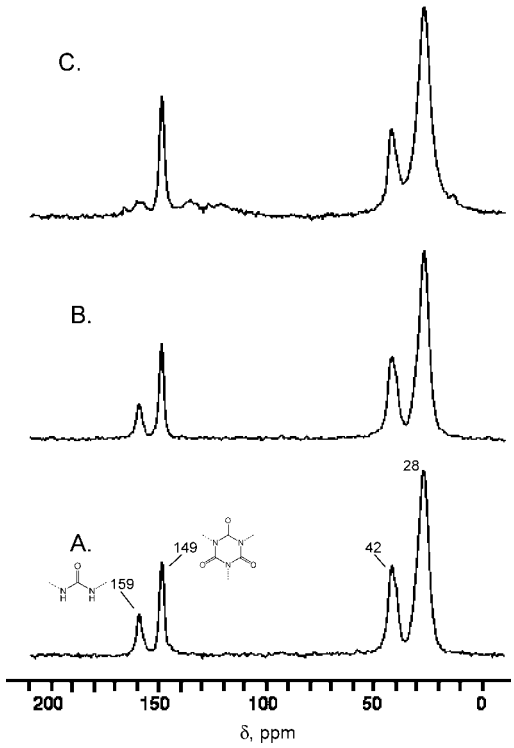

Figure 11. Solid ^{13}C CPMAS NMR of polyurea aerogels: (A) as-made, (B) after heating under Ar for 3 h at 250 °C, (C) after heating at 300 °C. After heating for 3 h under Ar at 200 °C, the spectrum was identical to the one of a sample as made. (For pertinent materials characterization data refer to Table 4.)

Scheme 3. First Decomposition Pathway of Polyurea Aerogels

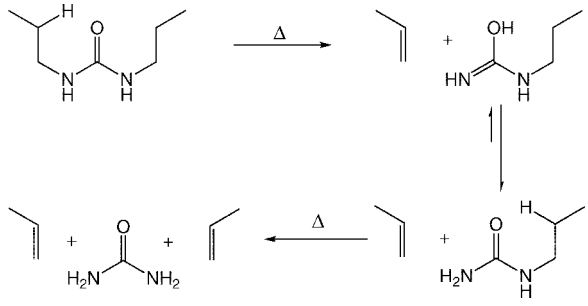

conclusions arrived at via eq 1. A second observation is that the aromatic carbon pattern in the 130−120 ppm range has changed dramatically: the intensity of the 120 ppm resonance has decreased and the whole pattern has become broader. Those changes are attributed to a direct involvement of the phenolic hydroxyls in reactions with the isocyanate to form carbamates. Changes observed in the carbonyl range 160−150 ppm are consistent with this argument: a new peak at 156 ppm can be explained by the newly formed carbamate carbonyls via reaction of isocyanates with phenolic hydroxyls on the surface of the RF nanoparticles. Phenolic C-OH carbons are not expected to move more than a couple of ppm by forming carbamates,[21] and thus the 152 ppm resonance is assigned to both kinds of aromatic C-OH and C-O-CO-NH- carbons. The shoulder at 148 ppm is again assigned to the isocyanurate carbonyls of N3300A. Overall, ^{13}C NMR confirms an increased uptake of polymer by using TEA as a cross-linking catalyst and indicates a higher degree of cross-linking involving more active sites on the skeletal framework. That in turn explains the lower shrinkage of X-RF aerogels prepared in the presence of TEA (Table 1). Similar results have been obtained by cross-linking with Desmodur N3200 in the presence of TEA (refer to the Supporting Information). Scheme 2 summarizes the cross-linking chemistry with and without TEA.

3.2. Preparation of Polyurea Aerogels. Results obtained by pyrolysis of X-RF aerogels (see section 3.3 below) render necessary an investigation of the behavior under similar conditions of the material derived by hydrolysis and condensation of Desmodur N3200 and N3300A by themselves. Thus, triethylamine was added as a catalyst in acetone/water solutions of Desmodur N3200 and Desmodur N3300A. Desmodur N3200 produced precipitates while solutions of N3300A gelled. Drying those gels from SCF CO_2 yields robust, opaque-white, low-density aerogels that shrink to about the same extent as the X-RF aerogels relative to their molds (∼20%), they maintain a high porosity (88%) and surface area (189 m^2 g^{-1}), and they consist of an entangled network of nanoworms (see Figure 5) very analogous to what has been observed with vanadia and templated silicas.[22,23] Table 2 summarizes the relevant material properties of those aerogels. Chemically, the material is polyurea (see section 3.4.1 below).

3.3. Pyrolysis of Native RF, X-RF, and Polyurea Aerogels. Figure 6 compares the thermogravimetric analysis data under inert atmosphere (N_2) of the three types of

(21) Albrecht, M.; Zauner, J.; Fröhlich, R.; Kataeva, O.; Wegejius, E.; Rissanen, K. *Synthesis* **2002**, *10*, 1434–1444.
(22) (a) Leventis, N.; Sotiriou-Levents, C.; Mulik, S.; Dass, A.; Schnobrich, J.; Hobbs, A.; Fabrizio, E. F.; Luo, H.; Churu, G.; Zhang, Y.; Lu, H. *J. Mater. Chem.* **2008**, *18*, 2475–2482. (b) Luo, H.; Churu, G.; Lu, H.; Schnobrich, J.; Hobbs, A.; Fabrizio, E. F.; Dass, A.; Mulik, S.; Leventis, N. *J. Sol-Gel Sci. Technol.* **2008**, *48*, 113–134.
(23) (a) Leventis, N.; Mulik, S.; Wang, X.; Dass, A.; Patil, V. U.; Sotiriou-Leventis, C.; Lu, H.; Churu, G.; Capecelatro, A. *J. Non-Cryst. Solids* **2008**, *354*, 632–644. (b) Leventis, N.; Mulik, S.; Wang, X.; Dass, A.; Sotiriou-Leventis, C.; Lu, H. *J. Am. Chem. Soc.* **2007**, *129*, 10660–10661.
(24) Silverstein, R. M.; Bassler, G. C.; Morrill, T. C., *Spectroscopic Identification of Organic Compounds*, 5th ed.; John Wiley & Sons: New York, 1991; Chapter 2.

Table 4. Pertinent Materials Characterization Data of Various Samples after Heat-Treatment under Ar at Three Different Temperatures As Indicated

aerogel type [heat-treated at]	bulk density[a] (ρ_b, g cm^{-3})	akeletal density[b] (ρ_s, g cm^{-3})	porosity, Π (% void space)[c]	BET surf. area, σ [avg pore diam.[d]] (m^2g^{-1} [nm])
native RF [200 °C]	0.146	1.379 ± 0.022	89	319 [19.8; 76.8]
native RF [250 °C]	0.125	1.404 ± 0.029	91	259 [31.6; 112]
native RF [300 °C]	0.127	1.387 ± 0.014	91	255 [33.4; 112]
polyurea [200 °C]	0.249	0.813 ± 0.011	69	[e]
polyurea [250 °C]	0.229	0.743 ± 0.007	69	[e]
polyurea [300 °C]	0.285	0.846 ± 0.024	66	[e]
X-RF-N3200 [200 °C]	0.610	1.267 ± 0.006	52	87.2 [26.5; 39.0]
X-RF-N3200 [250 °C]	0.656	1.059 ± 0.007	38	3.56 [26.9; 652]
X-RF-N3200 [300 °C]	0.385	1.109 ± 0.004	65	[e]
X-RF-N3300 [200 °C]	0.336	1.276 ± 0.006	74	171 [36.5; 51.3]
X-RF-N3300 [250 °C]	0.422	1.256 ± 0.016	66	16.1 [22.4; 391]
X-RF-N3300 [300 °C]	0.397	1.094 ± 0.040	64	14.3 [32; 449]

[a] Irregularly shaped samples; by the mercury displacement method [b] One sample, average of 50 measurements. [c] Porosity, $\Pi = [[1/(\rho_b) - 1/(\rho_s)]/(1/\rho_b)] \times 100$. [d] By the $4V_{Total}/\sigma$ method, where V_{Total} has been calculated by two methods, hence the two numbers cited for the average pore diameter: first automatically by the system software from a single point volume measurement of the N_2 adsorbed, and second manually from the bulk and skeletal densities via $V_{Total} = (1/\rho_b) - (1/\rho_s)$. [e] Isotherms show negative slopes and could not be used for surface area analysis.

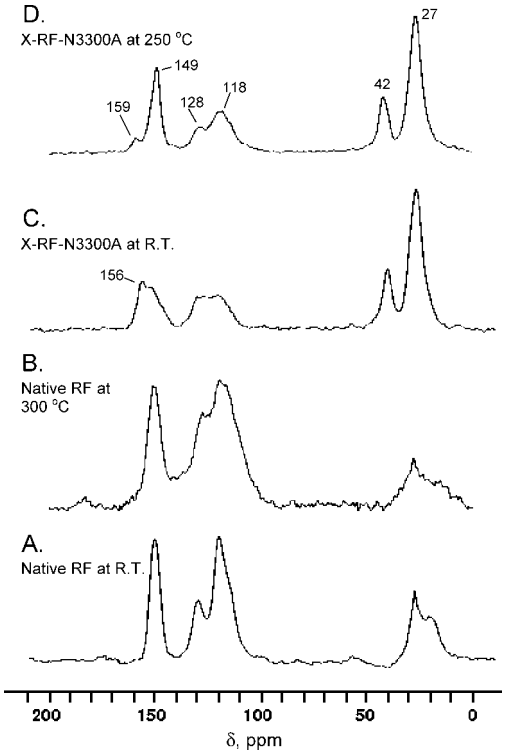

Figure 12. Solid ^{13}C CPMAS NMR of native RF and X-RF-N3300A aerogels after heat treatment under Ar at three different temperatures as indicated. The cross-linked sample after heat treatment at 250 °C does not loose the cross-linker (the high-field features maintain the same relative intensity) but it recovers features of the native RF aerogel, which is interpreted that the chemical bonding of the cross-linker with the polymer has been broken.

materials. Polyurea aerogels decompose almost completely above 500 °C yielding a ~5% w/w solid residue, and therefore mostly gaseous products. The onset of decomposition is around 300 °C. On the contrary, native RF aerogels yield a residue of about 20% of the original mass. X-RF samples behave similarly, yielding a residue of about the same mass as the native samples. No surprises up to this point. However, when those findings were translated into pyrolysis of large samples at 800 °C under Ar in a tube furnace in order to produce sizable carbon aerogel monoliths, it was realized that both the macroscopic and the microscopic appearance of the resulting materials were quite different. The tiny back flakes from pyrolysis of N3300A-derived polyurea are featureless, both macroscopically and microscopically, and consist of carbon (100% wt/wt by EDS). The black material obtained from pyrolysis of native RF aerogels comes in monolithic form, it is quite brittle, and dull (nonreflective; Figure 7). Microscopically, it looks identical to its native RF aerogel precursor (compare Figure 8A with Figure 1A). On the contrary, the black material from pyrolysis of X-RF aerogels cross-linked with N-3300A is much sturdier, glassy in appearance with metallic luster, and macroporous microscopically (Figures 7 and 8B). The material from pyrolysis of X-RF aerogels cross-linked with N-3200 is again extremely brittle, but it has metallic luster and its pores are visible to the naked eye (Figure 8C). All C-aerogels produced from native RF and X-RF aerogels consist exclusively of carbon (100% wt/wt by EDS). In XRD they show a very broad reflection with maximum at the graphite angle of $2\theta = 25°$ (see the Supporting Information). Again, N_2 adsorption isotherms do not reach saturation, but in conjunction with SEM (Figure 8), they should correspond to type IV isotherms for mesoporous materials (Figure 9A) and type II for macroporous materials (Figure 9B). The presence of an intermediate-pressure linear part (common in both type II and type IV isotherms) is formed by multilayer adsorption of N_2 on the pore walls and allows calculation of the surface area by the BET method. Material properties of all C-aerogels are summarized in Table 3. The porosites of C-aerogels from native versus X-RF aerogels are comparable, however, their BET surface areas are very different: the mesoporous C-aerogels from native RF aerogels have surface areas in the 600 m^2g^{-1} range (i.e., higher even than those of their parent RF aerogels), whereas the surface areas of the macroporous C-aerogels are much smaller: 17 m^2 g^{-1} for C-aerogels derived from X-RF-N3300A, and only 2.3 m^2 g^{-1} for C-aerogels derived from X-RF-N3200. Average pore diameters calculated by the $4V_{Total}/\sigma$ method agree well with the microscopic appearance of the materials. Similarly, particle size calculations show that the mesoporous material consists of nanoparticles about the same size as the parent native RF aerogels, whereas the *elementary building blocks* of the macroporous material (the term "particle" is not

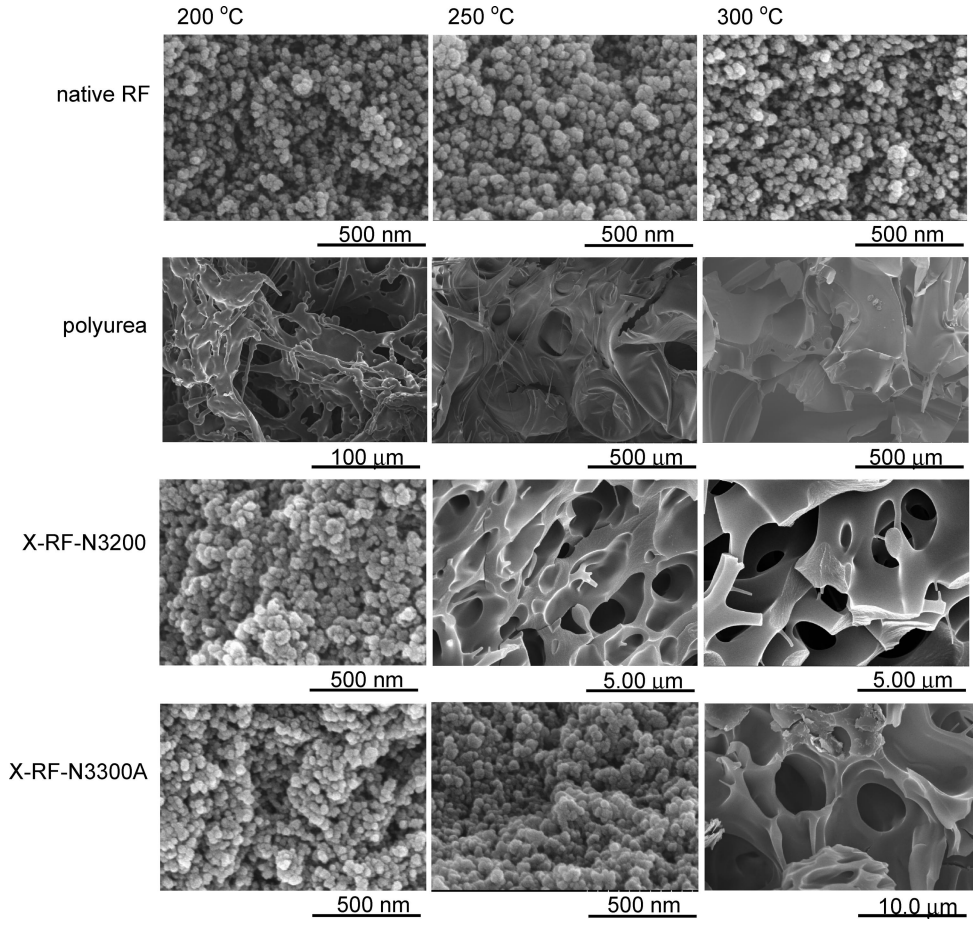

Figure 13. SEM of four types of aerogels, heat-treated under Ar for 3 h at three different temperatures, as indicated. (Notice the different magnifications and length scales. For pertinent materials characterization data, refer to Table 4.)

accurate in that case) are much larger. All C-aerogels are electrically conducting. The sheet resistance was measured with a four-point probe on flat surfaces produced by polishing larger monoliths with sand paper. Owing to their extreme fragility, that was not possible with C-aerogels from X-RF-N3200 samples. The bulk resistivity was calculated by multiplying the sheet resistance with the sample thickness and the results are cited in Table 3. Both macroporous and mesoporous C-aerogels are significantly more resistive than graphite (1375 $\mu\Omega$ cm). This is not surprising given the large fraction of their empty space. However, while the macroporous network is ~360 times more resistive than graphite, the mesoporous network is ~5000 times more so. At first approximation, the different conductivities of the two materials can be reconciled by the fact that in the mesoporous network the main contributor in the bulk resistance is the contact resistance between particles (Figure 8A), whereas in the macroporous network, the main contributor is the resistance of the skeletal filaments (Figure 8B). This model, however, is refined further in section 3.4.2 below.

3.4. Chemical, Physical, and Morphological Evolution of RF, X-RF, and Polyurea Aerogels upon Heat Treatment. The different morphology of C-aerogels resulting from pyrolysis of X-RF versus native RF aerogels is intriguing. Skeletal densities (Table 3) for the two types of aerogels are different, but all values are in the graphitic (2.267 g cm^{-3})/carbon black (1.8−2.1 g cm^{-3}) range indicating that the elementary building blocks in both kinds of materials are rather compact. Gases produced by decomposition of the cross-linker may account for the macropores. However, that mechanism alone would not account for the apparent lack of mesoporosity from the macroporous samples: gas evolution would account for the macropores but the surrounding walls should remain mesoporous. In order to investigate the mechanism that produces macropores, it was decided to follow the physical, chemical and morphological evolution of native RF, X-RF and polyurea aerogels upon heat treatment in the 200−300 °C temperature range that precedes and overlaps with the onset of the decomposition of the cross-linker (Figure 6).

3.4.1. Physical and Chemical Characterization after Heat Treatment at Different Temperatures. By DSC (Figure 10) N3300A-derived polyurea melts at 123 °C and starts decomposing above 280 °C, in agreement with TGA (Figure 6). Indeed, ^{13}C NMR (Figure 11) shows no chemical change between freshly made samples and samples treated up to 250 °C for 3 h under Ar. However, upon similar treatment at 300 °C, polyurea looses the urea carbonyl, presumably through a γ-hydrogen abstraction from both sides of the carbonyl in the mass-spectrometric McLafferty rearrangement fashion or a Norish type II photochemical cleavage.[24−26] In that regard, the broad resonances in the 120−130 ppm

(25) Barltrop, J. A.; Coyle, J. D. *Principles of Photochemistry*; John Wiley & Sons: New York, 1978; Chapter 6.

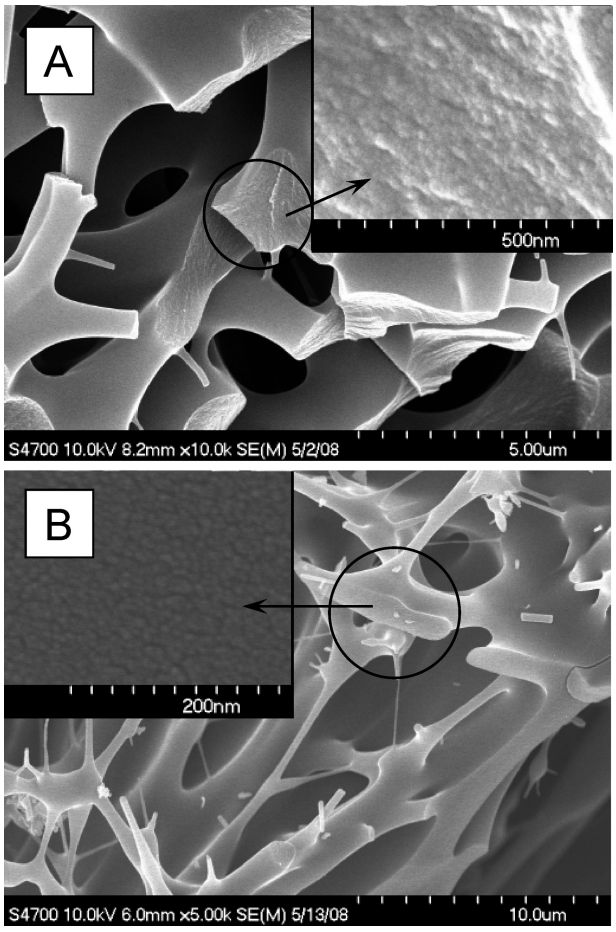

Figure 14. Looking inside the skeletal framework: (A) Survey SEM and SEM at the fracture (see inset) on the skeletal framework of an X-RF sample cross-linked with Desmodur N3200 (X-RF-N3200) and heat-treated under Ar at 300 °C (compare with A and notice the xerogel-like appearance inside the skeletal framework underneath the skin of molten cross-linker). (B) Survey SEM and SEM at the fracture (see inset) on the skeletal framework of a C-aerogel prepared by pyrolysis under Ar at 800 °C of a X-RF-N3300A aerogel. (Notice again the xerogel-like appearance inside the skeletal framework of the macroporous C-aerogel.)

range are assigned to terminal olefins produced by that decomposition pathway, consistent with previous reports (Scheme 3).[26] The isocyanurate ring (149 ppm) is heat-stable at least up to 300 °C.

By DSC, RF and X-RF aerogels (both with N3200 and N3300A) do not show any endotherms that would be evidence of melting. Instead, X-RF samples show signs of decomposition earlier than polyurea itself. Both N3200 and N3300A cross-linked samples start evolving heat at ~230 °C. Meanwhile, ^{13}C NMR shows that the RF skeletal framework is stable all the way up to 300 °C (compare spectra A and B in Figure 12). However, by 250 °C, X-RF samples cross-linked with N3300A (in the presence of TEA as catalyst) have lost the strong 156 ppm resonance (compare spectra C and D in Figure 12), which, as was mentioned above, has been assigned to carbamate cabonyls with phenolic hydroxyls (see section 3.1 above), and most importantly, the relative intensity of the peaks at 118/128 ppm has been restored back near to its native RF value (compare spectrum in Figure 12D with spectra in Figure 12A,B). At the same time, the cross-linker is still intact and remains within

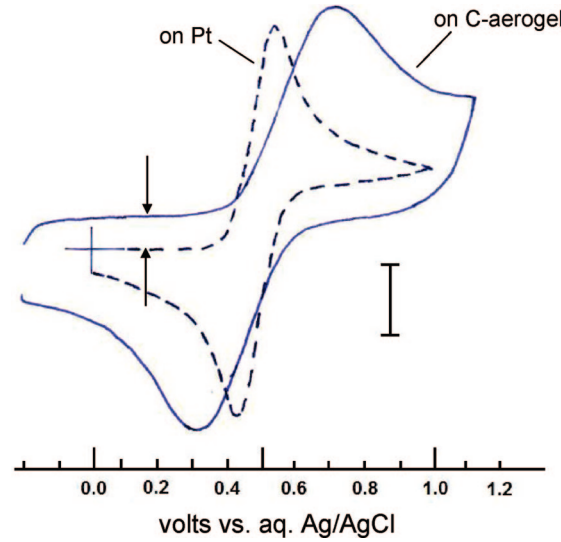

Figure 15. Cyclic voltammetry of ferrocene (3 mM) in CH_3CN/0.1 M TBAP at 0.1 V s^{-1}, using a Pt disk electrode (1 mm in diameter), or a C-aerogel electrode (0.008 g) made from a X-RF-N3300A aerogel, as indicated. Current scale: bar length 0.02 mA for Pt and 0.4 mA for the C-aerogel. (The C-aerogel surface area accessible by the electrolytic solution is calculated from the prewave charging current, shown with arrows.)

the sample as concluded by the low intensity urea carbonyl peak at 159 ppm and the relative intensity of the high-field feature (compare spectra C and D in Figure 12). Those data taken together suggest that the first step in the decomposition of the X-RF samples is at least some loss of the chemical bonding between the cross-linker and the RF backbone.

3.4.2 Morphological Characterization after Heat Treatment at Different Temperatures. Figure 13 presents the microscopic evolution (by SEM) of the three types of samples (native RF, X-RF, and polyurea) upon heat treatment at 200, 250, and 300 °C, and Table 4 summarizes the pertinent data. First, no significant morphological change is observed in the native RF samples in agreement with ^{13}C NMR (Figure 12). At all three temperatures, samples retain their nanoparticulate structure, although in general the secondary particles should be coming closer together, as reflected on both the porosity and the surface area, which have been both steadily reduced (compare Tables 1 and 4). On the other hand, Desmodur N3300A derived polyurea has already melted at 200 °C, losing its nanowormlike morphology. Macroporous voids appear as early as 200 °C, and by 250 °C polyurea samples closely resemble those of C-aerogels obtained after pyrolysis of X-RF-N3300A aerogels at 800 °C. By 300 °C, polyurea aerogels have collapsed completely to the same featureless solid observed after their pyrolysis at 800 °C. Because by TGA and ^{13}C NMR no significant decomposition, and therefore no significant gas evolution, has taken place off polyurea samples at 250 °C, we conclude that the macropores are caused by the surface tension forces developing during melting. Now, from that perspective, none of the X-RF samples melts (by DSC, Figure 10) or changes its appearance otherwise after heat-treatment up to 200 °C. At 250 °C, X-RF-N3200 samples have melted, whereas X-RF-N3300A samples remain intact.

(26) Durairaj, B.; Dimock, A. W.; Samulski, E. T. *J. Polym. Sci., Part A: Polym. Chem.* **1989**, *27*, 3211–3225.

(27) Svec, F.; Huber, C. G. *Anal. Chem.* **2006**, *78*, 2101–2107.

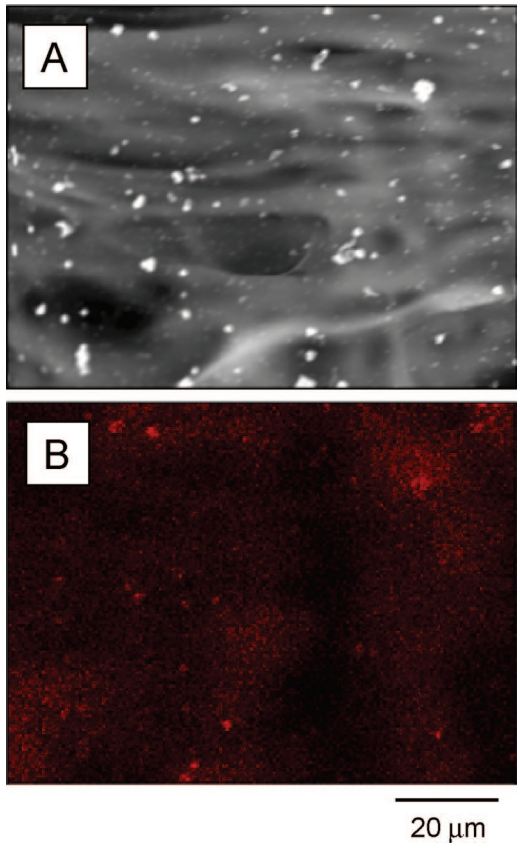

Figure 16. (A) SEM of a carbon aerogel prepared by pyrolysis of a X-RF-N3300A aerogel after electrodeposition of Pt from a 3 mM solution of K_2PtCl_4 in CH_3CN/0.1 M TBAP containing enough water to solubilize the salt. (B) energy-dispersive spectra (EDS)-derived Pt map at the same location.

By 300 °C, both kinds of X-RF samples have melted, acquiring macroporous morphologies similar to those of their terminal C-aerogels after pyrolysis at 800 °C. (It is pointed out, however, that none of the samples pyrolyzed up to 300 °C is electrically conducting. Electrical conductivity appears upon pyrolysis above 600 °C.)

From the above, decomposition and gas evolution are not the main factors that create the macropores, simply because creation of macropores precedes those processes. The melt-and-flow model seems to explain adequately the macroporosity in C-aerogels from X-RF aerogels. However, that model is only a first approximation. For example, if we consider the thermal stability of native silica versus native RF aerogels, we realize that although the skeletal frameworks of both materials are stable up to 300 °C, nevertheless, X-RF aerogels cross-linked with N3200 show complete melting at 250 °C (Figure 13) in contrast to silica aerogels cross-linked with Desmodur N3200 that do not show any signs of melting up to 300 °C (see the Supporting Information). Therefore, the different behavior of the two cross-linked materials (silica and RF) has to be attributed to the chemical interaction of the cross-linker with the skeletal framework. The cross-linker is covalently bonded to the skeletal framework, and in essence the assembly comprises a new chemical entity with its own physical and chemical properties. Consistent with the DSC and ^{13}C NMR data, it seems that as the temperature increases the urethane bridges between RF and the cross-linker break first. Because N3200 (a diisocyanate) has fewer points of attachment to the RF network than N3300A (a triisocyanate), the separation of the cross-linker from the RF framework is more efficient and it occurs quantitatively at lower temperatures (250 °C versus 300 °C). The released polymer finds itself above its melting point, wetting and causing collapse of the surrounding framework. Again, with fewer points of attachment to the RF framework, this process is more effective with N3200, causing probably more extended collapse and larger pores. Cross-sections of the X-RF-N3200 framework after heat-treatment at 300 °C (Figure 14.A, Inset) show nanoparticles squeezed close together into a xerogel-like structure covered with a smooth skin from the melted cross-linker. The same morphology is retained within the walls surrounding the macropores after pyrolysis of X-RF-N3300A aerogels at 800 °C (Figure 14B, inset) The xerogel-like internal texture of the macroporous walls of C-aerogels is consistent with the lower skeletal densities of those materials relative to the skeletal densities of C-aerogels from native RF. Furthermore, the better contact between carbon particles squeezed together in a xerogel-like fashion also explains the lower resistivity of our macroporous variety of C-aerogels.

4. Electrochemical Evaluation of C-Aerogels Made from X-RF Aerogels

It is well-established from work in monolithic separation media that mass transfer in macropores has both convective and diffusional components, while only diffusion prevails in mesopores.[27] That, coupled with the fact that our macroporous carbon aerogels are more electrically conducting than typical mesoporous C-aerogels, suggests that sturdy macroporous C-aerogels may be useful as gas diffusion electrodes in fuel cells. In that regard, the actual performance of macroporous C-aerogels as electrode materials was evaluated electrochemically. Figure 15 compares the cyclic voltammograms of ferrocene on a monolithic macroporous C-aerogel electrode made from X-RF-N3300A versus on a typical Pt disk electrode. The large prewave background current, $i_{background}$, in the C-aerogel electrode is due to charging of the double layer, and on the basis of the relationship $i_{background} = \nu C_d$ (ν is the potential sweep rate, set equal to 0.1 V s^{1-}), we calculate the double layer capacity, C_d. [28] Assuming a typical value for the specific electrical double layer capacity of 20 μF cm^{-2},[28] it is calculated that the electrode area is in the order to 1.25 m^2 g^{-1}. This figure is lower than the BET surface area reported in Table 3 for the same material (17 m^2 g^{-1}), and the difference is taken as evidence that the electrolytic solution does not reach all surfaces accessible for N_2 physisorption, or equivalently, only a fraction of the BET surface area is accessible for redox chemistry. A second observation is that the potential peak-to-peak separation, E_{p-p}, is much larger with the C-aerogel electrode (390 mV) than what it is with Pt (100 mV) and that is attributed directly to the higher ohmic resistance of the carbon electrode. Because of their fragility, it was difficult to conduct similar experiments with C-aerogels derived from either native RF or X-RF-N3200 aerogels.

(28) Bard, A. J.; Faulkner, L. J. *Electrochemical Methods, Fundamentals and Applications*, 2nd ed.; John Wiley & Sons: New York, 2000.

Macroporous C-aerogels from X-RF-N3300A were finally used as substrates for the electrochemical deposition of Pt, which is used as catalyst in fuel cell electrodes. The electrocatalytic activity of those materials will be reported elsewhere. Figure 16A shows a low-resolution SEM after Pt electrodeposition, and Figure 16B shows the EDS-generated Pt map on the same spot. The charge consumed for electrodeposition of Pt was 85.6 mC, corresponding to 4.44×10^{-4} mmol of Pt. The piece of C-aerogel used as an electrode weighed 0.046 g, and by considering the BET surface area from Table 3 (17 m^2 g^{-1}), it is calculated that the specific electrode had a total internal surface area (both accessible and inaccessible electrochemically) of 0.782 m^2. Therefore, the Pt coverage was 5.67×10^{-11} mol cm^{-2}, which corresponds to 57% of a monolayer coverage (assuming 1.0×10^{-10} mol cm^{-2} for a single monolayer coverage with a small molecule). However, as can be seen on the Pt map, the metal has been deposited nonuniformly, but rather in islands.

5. Conclusions

Polymer cross-linked RF aerogels are sturdier and lower density materials than their corresponding native RF precursors, and therefore they may be pursued on their own right for typical aerogel applications in thermal and acoustic insulation. Pyrolysis of those materials, however, creates directly a new class of macroporous carbon aerogels, without a need for templating agents, as the common practice has been so far in the literature. The mechanism of macropore formation is a fortuitous combination of (a) chemical stability of both the RF framework and the cross-linker up to 300 °C; (b) cleavage of the RF-cross-linker covalent bonding at lower temperatures than what is required for decomposition of the cross-linker; and (c) a low melting point for the latter. The new materials are electrically conducting and they appear promising for application as fuel cell electrodes. Importantly, along the way, we have encountered a quite interesting method of producing low-density polyurea aerogels by the in situ generation of amines via hydrolysis of isocyanates. The latter materials are currently evaluated structurally, chemically, thermally, and mechanically.

Acknowledgment. We acknowledge the University of Missouri Research Board (N.L.) and the NSF under CHE-0809562 and CMMI-0653919 for financial support. We also thank Dr. Wei Wycoff for her assistance with solids NMR and Professor Douglas K. Ludlow for his assistance with N_2 sorption porosimetry.

Supporting Information Available: FTIR spectra of RF and X-RF aerogels. Solid CPMAS ^{13}C NMR spectra of X-RF aerogels cross-linked with Desmodur N3200. XRD of carbon aerogels from native and X-RF aerogels. SEM after heat treatment at three different temperatures of silica aerogels cross-linked with Desmodur N3200 (PDF). This material is available free of charge via the Internet at http://pubs.acs.org.

CM801428P